ACS APPLIED MATERIALS & INTERFACES

Research Article

www.acsami.org

Effect of Geometric Nanostructures on the Absorption Edges of 1-D and 2-D TiO_2 Fabricated by Atomic Layer Deposition

Yung-Huang Chang,[†] Chien-Min Liu,[†] Hsyi-En Cheng,[‡] and Chih Chen*,[†]

[†]Department of Materials Science and Engineering, National Chiao Tung University, Hsin-chu 30010, Taiwan, Republic of China

[‡]Department of Electro-Optical Engineering, Southern Taiwan University of Science and Technology, Tainan 710, Taiwan, Republic of China

ABSTRACT: 2-Dimensional (2-D) TiO_2 thin films and 1-dimensional (1-D) TiO_2 nanotube arrays were fabricated on Si and quartz substrates using atomic layer deposition (ALD) with an anodic aluminum oxide (AAO) template at 400 °C. The film thickness and the tube wall thickness can be precisely controlled using the ALD approach. The intensities of the absorption spectra were enhanced by an increase in the thickness of the TiO_2 thin film and tube walls. A blue-shift was observed for a decrease in the 1-D and 2-D TiO_2 nanostructure thicknesses, indicating a change in the energy band gap with the change in the size of the TiO_2 nanostructures. Indirect and direct interband transitions were used to investigate the change in the energy band gap. The results indicate that both quantum confinement and interband transitions should be considered when the sizes of 1-D and 2-D TiO_2 nanostructures are less than 10 nm.

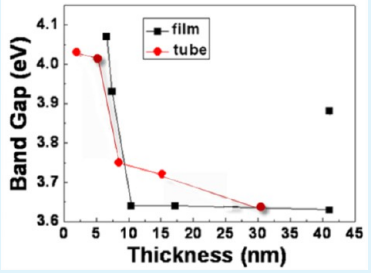

KEYWORDS: *2-D TiO_2 thin films, 1-D TiO_2 nanotube arrays, quantum confinement, interband transitions, atomic layer deposition, anodic aluminum oxide*

INTRODUCTION

Nanostructured materials, such as quantum dots,[1] nanorods,[2] nanowires,[3] nanotubes,[4−6] nanobelts,[7] and nanopores[8−10] have attracted much interest due to their potential in various applications. From among the many nanostructured materials, TiO_2 nanostructures have emerged as one of the most promising materials for optoelectronic devices due to their variety of growth methods, high melting point of 1855 °C, thermal and chemical stability at high temperatures, wide and indirect semiconductor band gap, and high photoconversion efficiency and photostability.[11−24] As reported in the literature,[25−30] a blue-shift phenomenon was observed for the absorption edge with decreasing TiO_2 nanoparticle size. Depending on the fabrication process, the onset of the blue-shift for TiO_2 nanoparticles is exhibited for a diameter of approximately 1−10 nm.[26,31−34] This phenomenon is not yet clearly understood. Some researchers have proposed that the blue-shift was due to the quantum size effect,[31] also called quantum confinement, and some proposed that the shift was due to direct interband transitions.[26,29] According to the theory based on quantum confinement, when the size of the nanoparticles approaches the Bohr radius, the continuous bands break down and the energy levels become discrete, resulting in a higher energy band gap and in the blue-shift phenomenon. The two factors that can influence the Bohr radius include the dielectric constant and the effective mass of electrons and holes. These values change for different fabrication conditions and measuring devices, especially the effective mass of electrons and holes on the nanoscale. Therefore, the Bohr radius is different for different nanostructures. Generally, regardless of the variation in the dielectric constant and in the effective mass of electrons and holes, the Bohr radius of TiO_2 is from 1 to 10 nm.[26,31−34] According to the theory based on direct interband transitions, Serpone et al.[26] proposed that the low-energy indirect interband transition might be replaced by a direct interband transition, depending on the particle size and on the surface environment. Although the blue-shift phenomenon is still under investigation, it is well-known that the optical absorption characteristics can be altered by modifying the geometry of the nanoparticles, such as the thickness of the films or of the nanotube walls.

Although the quantum size effect and direct interband transitions were proposed as reasons for the blue-shift in the absorption edge, only a few researchers have investigated this shift using these two theories for both 2-dimensional (2-D) and 1-dimensional (2-D) nanostructures. Therefore, in this study, we prepared 2-D TiO_2 thin films and 1-D TiO_2 nanotube arrays using an anodic aluminum oxide (AAO) template and atomic layer deposition (ALD) technology at 400 °C to investigate the relation between the absorption edge and the energy band gap. The effects of the geometric nanostructures on the absorption edge and the mechanism of the indirect and direct interband transitions are discussed.

EXPERIMENTAL SECTION

First, AAO was prepared on Si and quartz substrates. A 1 μm Al film, which served as the AAO layer, was deposited onto the substrates using a thermal evaporation coater according to a fabrication

Received: October 10, 2012
Accepted: April 10, 2013
Published: April 10, 2013

procedure from a previous study.[35] The substrates with AAO were then placed in a quartz tube reactor that was maintained at 1.6×10^{-1} Torr and at 400 °C. $TiCl_4$ and $H_2O_{(g)}$ (deionized water) precursors, which were separately kept in canisters at 30 ± 1 and 25 ± 1 °C, were used as Ti and O sources. Pure Ar gas (99.999%) was used as a carrier gas and as a purge gas. Each deposition cycle consisted of the following eight steps: $TiCl_4$ reactant addition, pump down, Ar purge, pump down, H_2O reactant addition, pump down, Ar purge, and pump down. The typical pulse time used to introduce the $TiCl_4$ and H_2O precursors was 1 s, and the Ar purge time was also 1 s. To efficiently remove any residual reactants and byproducts, a 1 s pump down step was added after each step. Deposition cycles with 50, 100, 200, 300, and 700 cycles were chosen to produce various thicknesses of the TiO_2 nanostructures.

The nanostructures of the TiO_2 materials were examined using a field emission scanning electron microscope (FESEM, JSM-6500F) and a transmission electron microscope (TEM, JEM-2100F). X-ray diffraction (XRD) was adopted to analyze the structure of the TiO_2 films and nanotubes. A UV−vis spectrometer (U-3500, Hitachi) was utilized to measure the absorption characteristic of the TiO_2 thin films and nanotubes on quartz substrates.

RESULTS AND DISCUSSION

Figure 1 shows the FESEM images of the TiO_2 thin films for 50, 100, 200, 300, and 700 deposition cycles. The surfaces of the thin films consisted of crystalline structures, and the grain sizes increased with increasing film thickness.[36] When the number of deposition cycles was small, the sizes of the nanoparticles were uniform, as shown in Figure 1a−d. However, as the number of deposition cycles increased, the nanoparticle size became nonuniform, as shown in Figure 1e. As measured from the TEM cross sections of the TiO_2 thin films, not shown here, the thicknesses of the thin films were 6.6, 8.1, 12, 18.2, and 41.1 nm. The average growth rate is 0.054 nm/cycle by fitting thin film thicknesses from 50 to 700 cycles.[36] Figure 2 presents the film thickness as a function of deposition cycle. The fitting curve was also plotted in the figure. The fitting curves did not pass through 0 nm at 0 cycles. This means that the initial deposition rate during the first few cycles is faster than that during the later growth. This may be attributed to the precursors possibly having better adsorption on the SiO_2 and AAO surfaces. Once the surfaces were covered by crystalline TiO_2, the adsorption of the precursors may become slightly worse.[16] Therefore, the growth rate in the very initial stages was faster than that in later stages.

Figure 3a−e shows the TEM cross sections of the TiO_2 nanotubes on an AAO template for 50, 100, 200, 300, and 700 deposition cycles. Using the cross-sectional TEM images, the tube wall thicknesses were measured to be 3.0, 5.3, 8.5, 15.2, and 30.7 nm for 50, 100, 200, 300, and 700 deposition cycles, respectively.[36] The calculated growth rate is 0.043 nm/cycle by fitting tube wall thicknesses from 50 to 300 cycles, as shown in Figure 2. The TEM images show that ALD can be used to precisely control the TiO_2 tube wall thickness by changing the number of deposition cycles. Figure 3a shows the TEM image of TiO_2 deposited separately on a SiO_2 native oxide and on AAO tube walls after 50 deposition cycles. The TiO_2 layer appeared to be thicker on the native oxide than on the AAO tube walls. We also observed that the TiO_2 deposited on the native oxide exhibited a crystalline structure, while the TiO_2 deposited on the AAO tube walls did not. This result might indicate that the precursors, $TiCl_4$ and H_2O, had high enough energies to overcome the barrier height when they were deposited on the native oxide, thus forming crystalline structures and thicker films after the reaction at 400 °C. Figure

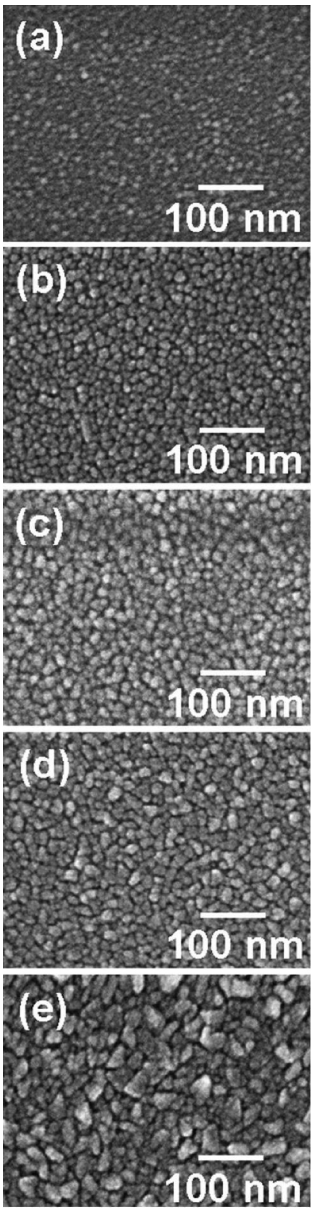

Figure 1. FESEM top views of the TiO_2 thin films deposited at 400 °C after (a) 50, (b) 100, (c) 200, (d) 300, and (e) 700 deposition cycles.

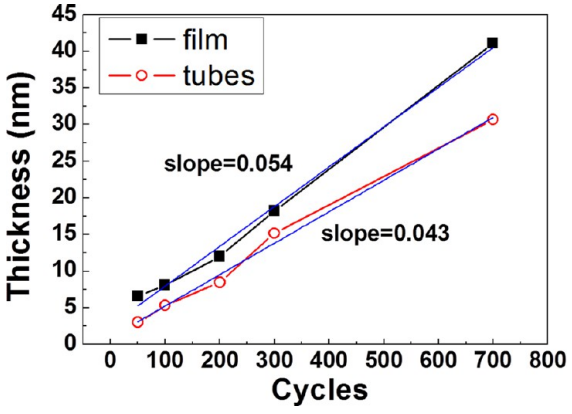

Figure 2. Plot of TiO_2 thickness as a function of deposition cycle for both ALD films and tubes. Linear fitting lines were also shown in the figure.

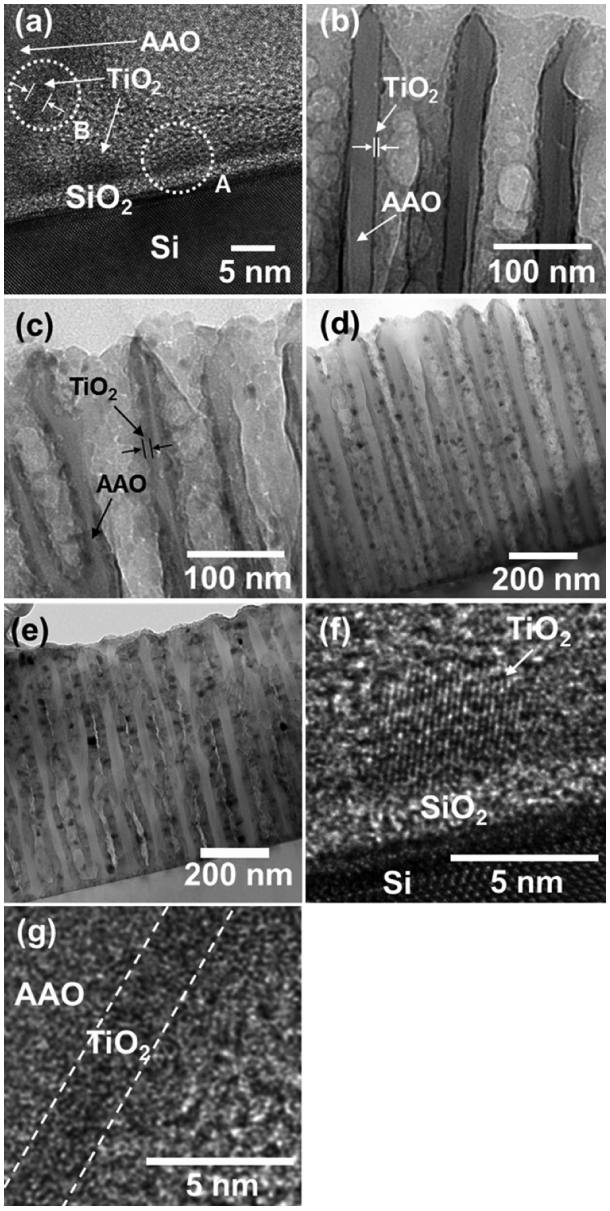

Figure 3. TEM cross sections of the TiO_2 nanotubes with an AAO template at 400 °C after (a) 50, (b) 100, (c) 200, (d) 300, and (e) 700 deposition cycles. (f and g) The high resolution TEM image of the dotted circle A and B shown in (a), respectively. After 50 deposition cycles at 400 °C, a crystalline TiO_2 nanostructure was clearly observed on the surface of the native oxide.

3f,g shows the high resolution TEM images of the dotted circular area A and B in Figure 3a, respectively. From Figure 3f, a crystalline TiO_2 nanostructure that grew on the surface of the native oxide was clearly observed and its size is about 3.3 nm in thickness. On the other hand, the amorphous structure of the TiO_2 on the AAO was confirmed in Figure 3g. Furthermore, the XRD patterns in Figure 4a,b show the evolution of nanostructures for the thin films and the nanotubes at different deposition cycles, respectively. On the basis of the XRD patterns, the TiO_2 thin films and nanotubes are both identified as an anatase structure. No peaks below 100 cycles could be attributed to the crystalline films being too thin to be detected by XRD. A detailed characterization of TiO_2 thin films and of TiO_2 nanotube arrays was described in an earlier report.[16,36]

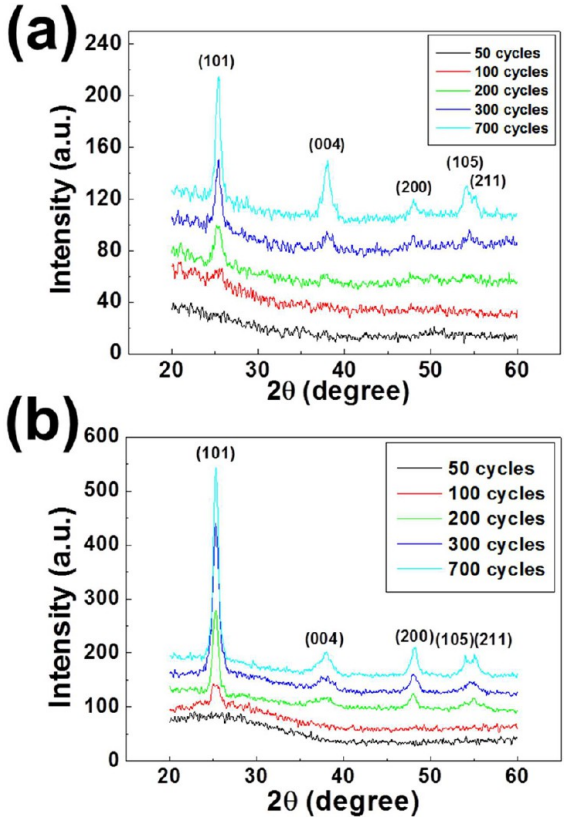

Figure 4. XRD patterns showing the structure evolution for the nanostructures at different deposition cycles: (a) thin films TiO_2 and (b) nanotubes TiO_2.

Figure 5 shows the absorption spectra of the TiO_2 thin films and nanotube arrays. The TiO_2 thin films and the TiO_2 nanotube arrays are transparent in the visible wavelength region, as shown in Figure 5a,b. The onset of the absorbance behavior occurs at wavelengths from 350 to 380 nm, except for the 700 cycle deposition due to a broader onset range. This broad onset range was also observed by Serponen et al. and by Wang et al.[26,34] Serpone suggested that this phenomenon could be attributed to the formation of colloidal TiO_2 in a complex process. However, Wang proposed that the difference in absorption wavelength indicates a difference in the band gap of TiO_2 with increasing loading of the inorganic phase. The absorbability increased with increasing film and tube wall thicknesses. Additionally, a blue-shift in the absorption edge[25,30] was observed for thinner films and thinner tube walls, especially for 1-D nanotube arrays. According to the literature,[37,38] this phenomenon is attributed to the continuous bands breaking down and to the energy levels becoming discrete, becoming a quantum state, when a material is on the nanoscale. Therefore, a blue-shift in the absorption edge was more obvious for 1-D nanotubes than for 2-D thin films, as shown in Figure 5a,b.

An absorption spectrum represents the energy required for electrons to be excited from the valence band to the conduction band. Therefore, the band gap energy, E_g, can be determined from the absorption coefficient near the absorption edge. The equation for indirect interband transitions is as follows:[26,27]

$$\alpha = B_i(h\nu - E_g)^2/h\nu \quad (1)$$

dx.doi.org/10.1021/am302219n | ACS Appl. Mater. Interfaces 2013, 5, 3549−3555

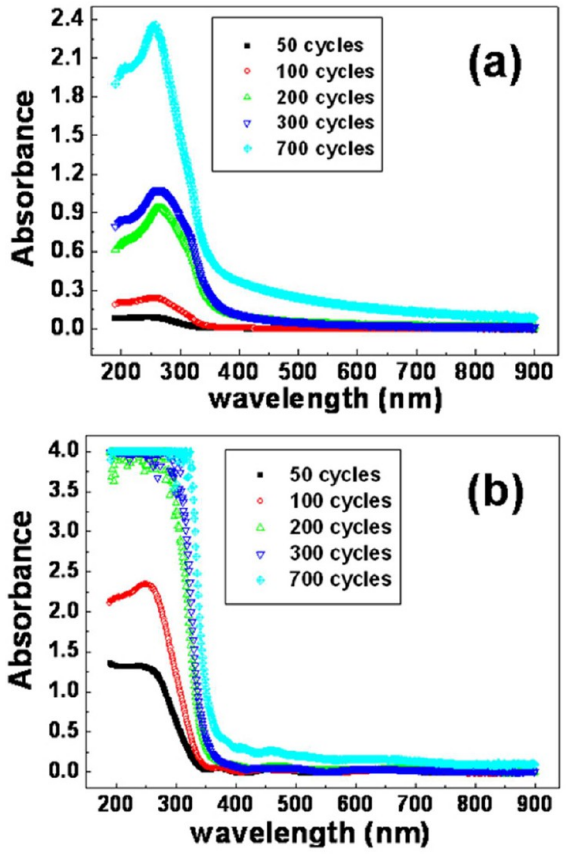

Figure 5. Absorption spectra of (a) the TiO_2 thin films and (b) the TiO_2 nanotube arrays for 50, 100, 200, 300, and 700 deposition cycles.

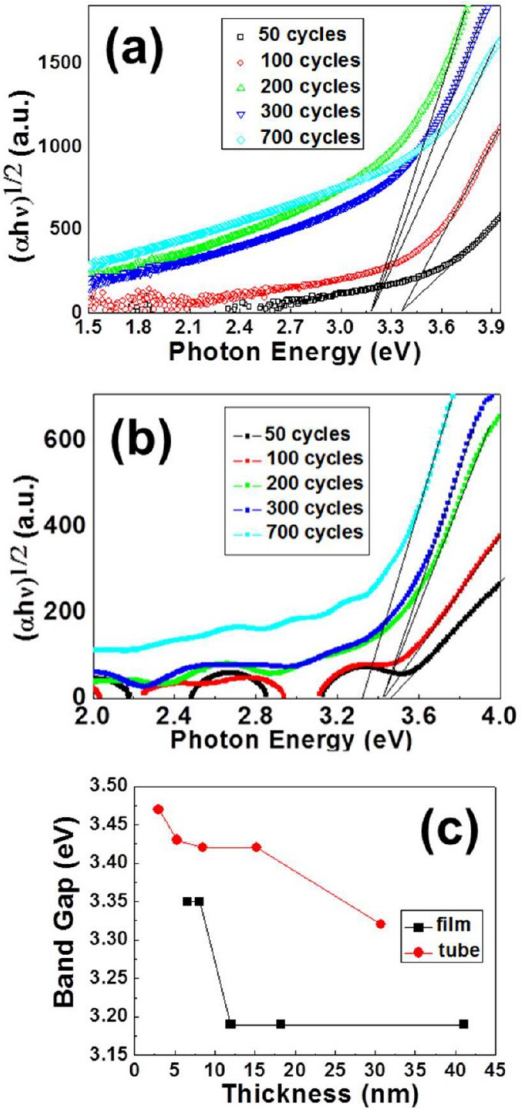

Figure 6. Plots of $(\alpha h\nu)^{1/2}$ versus the photon energy ($h\nu$) from the spectra of the indirect interband transitions of (a) the TiO_2 thin film and (b) the TiO_2 nanotubes, whose linear fit intercepts represent the band gap energy. (c) Band gap energies of the TiO_2 thin film and nanotubes for different film and wall thicknesses.

where α is the optical absorption coefficient near the absorption edge, B_i is the absorption constant for an indirect transition, and $h\nu$ is the incident photon energy. Figure 6a,b shows the plots of $(\alpha h\nu)^{1/2}$ versus the photon energy ($h\nu$) for indirect interband transitions in TiO_2 thin films and nanotubes. From the spectra, we obtain linear fit intercepts of 3.35, 3.35, 3.19, 3.19, and 3.19 eV for TiO_2 thin film and of 3.47, 3.43, 3.42, 3.42, and 3.32 eV for TiO_2 nanotubes for 50, 100, 200, 300, and 700 deposition cycles. Figure 6c shows the band gap energies corresponding to different TiO_2 thin film and nanotube wall thicknesses for different deposition cycles. As mentioned earlier, according to the theory of quantum confinement, when a material approaches the size of its Bohr radius, the energy levels become discrete, and the band gap energy increases. The Bohr radius[28] can be determined from:

$$a_B = 4\pi\varepsilon_r\varepsilon_0\hbar^2/\mu e^2 \quad (2)$$

where ε_r is the dielectric constant ($\approx$30–185), ε_0 is the permittivity of free space, $\mu = [1/m_e^* + 1/m_h^*]^{-1}$ is the effective mass of electrons and holes, and e is the charge of an electron.[39,40] The m_e^* value ranges from 5 to 30 m_0, and the m_h^* value ranges from 0.01 to 3.0 m_0.[39,41] The dielectric constant and the effective mass of electrons and holes are the two most important factors that can influence the Bohr radius. These two factors are highly variable due to fabrication conditions and to the nanoscale size. To simplify the issue, the variations in the dielectric constant and in the effective mass of the electrons and holes are disregarded. Therefore, the Bohr radius of TiO_2 should be between 1 and 10 nm.[26,31−34]

As shown in Figure 6c, the band gap energy increases when the thicknesses of the TiO_2 thin films and of the TiO_2 nanotubes are less than 10 nm. This phenomenon appears to be due to quantum confinement. However, a change in the band gap energy is also observed when the thickness of the TiO_2 nanotubes is larger than 10 nm. When the radius of a particle is equal to or smaller than the Bohr radius, the quantum confinement effect increases the band gap energy. The increase in the energy can be expressed as:[26,28]

$$\Delta E_g = \frac{h^2}{8\mu R^2} - \frac{1.8e^2}{4\pi\varepsilon_o\varepsilon_r R} \quad (3)$$

where R is the radius of the particle. Figure 7 shows the plot of ΔE_g, obtained from eq 3 and from the experimental results, vs the film or tube wall thicknesses. The theoretical values of ΔE_g are obtained using $\mu = 0.05$ and $\varepsilon_r = 75$, as reported by King et al.[28] The experimental values of ΔE_g are obtained by deducting the bulk material E_g value of 3.19 eV from the E_g values

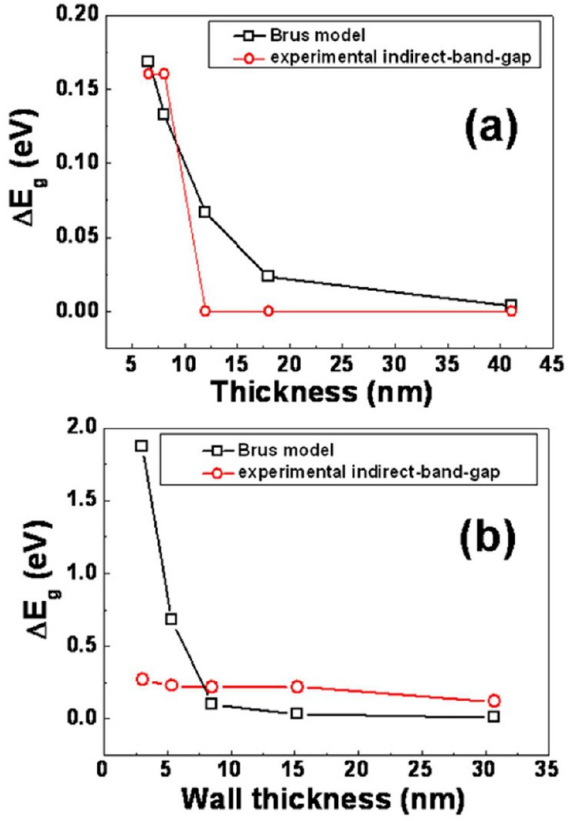

Figure 7. Plots of ΔE_g vs the thicknesses of (a) the TiO_2 thin films and (b) the TiO_2 nanotube walls based on eq 3 and on the experimental results.

determined above. As shown in Figure 7a,b, the theoretical and experimental values are similar for the TiO_2 thin films but are not similar for the TiO_2 nanotubes. This result indicates that, when the thickness of the thin films is in the range of 6.6 to 12 nm, the change in the band gap energy can be explained by quantum confinement. Although the band gap energy of the nanotubes still increases with decreasing wall thickness, as shown in Figure 6c, this increase is not as drastic as that from the theory when the wall thickness is less than 10 nm. It was expected that the 1-D nanotubes would be closer to a quantum state than the 2-D thin films. Therefore, it is hard to completely explain the change in the band gap energy of 1-D TiO_2 nanotubes using the quantum size effect.

We analyze the band gap energy based on the theory of direct interband transitions using the absorption spectra shown in Figure 5. The equation for the absorption coefficient is as follows:[26]

$$\alpha = B_d(h\nu - E_g)^{1/2}/h\nu \quad (4)$$

where α is the optical absorption coefficient near the absorption edge and B_d is the absorption constant for a direct transition. Figure 8a shows a plot of $(\alpha h\nu)^2$ versus the photon energy $(h\nu)$ for the direct interband transitions of the TiO_2 thin film. The linear fit intercepts are 4.07, 3.93, 3.64, and 3.64 eV for 50, 100, 200, and 300 deposition cycles, respectively. For the 700 cycle TiO_2 thin film, there are two linear fit intercepts at 3.63 and 3.88 eV. Two intercepts were reported by Serpone et al.[26] at 2.97 and 3.21 eV for colloidal anatase TiO_2 particles under a similar situation. As shown in Figure 8b, the linear fit intercepts for 50, 100, 200, 300, and 700 cycle TiO_2 nanotubes were

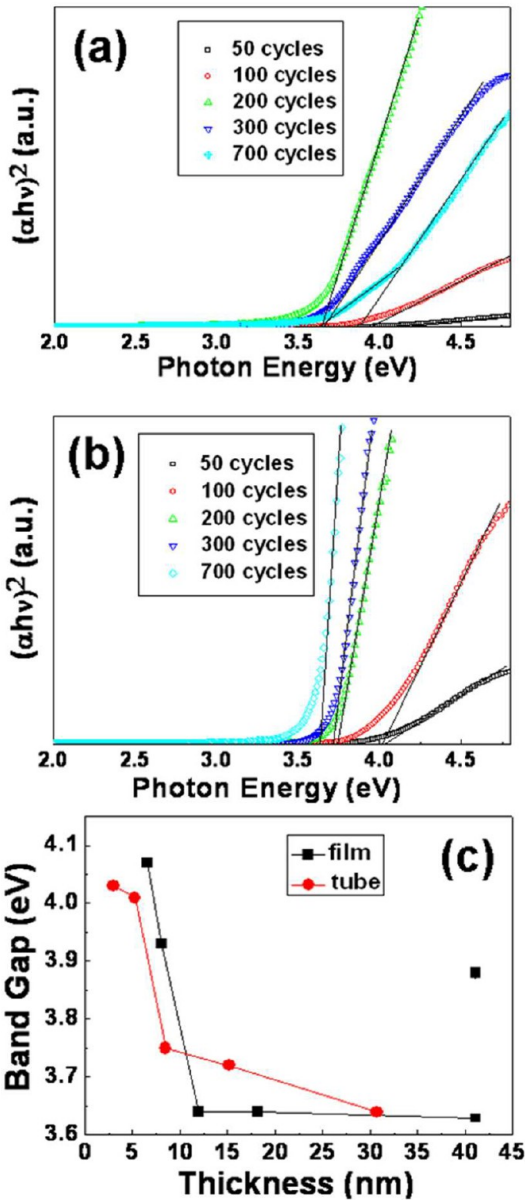

Figure 8. Plots of $(\alpha h\nu)^2$ versus the photon energy $(h\nu)$ from the spectra of the direct interband transitions of (a) the TiO_2 thin film and (b) the TiO_2 nanotubes, whose linear fit intercepts represent the band gap energy. (c) Band gap energies of the TiO_2 thin film and nanotubes for different thicknesses.

estimated as 4.03, 4.01, 3.75, 3.72, and 3.64 eV, respectively. Figure 8c shows the plot of the band gap energy vs the TiO_2 thin film and nanotube wall thicknesses for different deposition cycles. Because the onset of the absorption edge is determined by the lowest direct interband transition, there must be a corresponding energy level for the transitions of the excited electrons. On the basis of the energy level diagram,[25,42] $X_2 \rightarrow X_1$ and $\Gamma_{5'} \rightarrow \Gamma_1$ belong to direct interband transitions with band gap energies of 3.59 and 4.05 eV, respectively. The corresponding values of $X_2 \rightarrow X_1$ are 3.64, 3.64, and 3.63 eV for the TiO_2 thin film and 3.75, 3.72, and 3.64 eV for the TiO_2 nanotubes for 200, 300, and 700 deposition cycles. The corresponding values of $\Gamma_{5'} \rightarrow \Gamma_1$ are 4.07 and 3.93 eV for the TiO_2 thin film and 4.03 and 4.01 eV for the TiO_2 nanotubes for the 50 and 100 deposition cycles. Although the corresponding

dx.doi.org/10.1021/am302219n | ACS Appl. Mater. Interfaces 2013, 5, 3549−3555

energy levels of $X_2 \rightarrow X_1$ and $\Gamma_{5'} \rightarrow \Gamma_1$ can be determined (especially for nanotubes less than 10 nm in diameter), different transition levels are not expected for the onset of the absorption edge. Furthermore, it was noticed that the band gap energy increased with decreasing thickness when the thickness of films or of the nanotubes was less than 10 nm. Therefore, the shift in the absorption edge and the increase in the band gap energy cannot be completely explained by the theory of direct interband transitions either. Additionally, on the basis of our experimental results, shown in Figure 6c, the 1-D tubular nanostructures have a higher band gap energy than the 2-D planar nanostructures. This result indicates that the variations in the geometric nanostructures of the 1-D and 2-D materials induce the separation of the band, resulting in the blue-shift of the absorption edges. In summary, it appears that no single theory, either quantum confinement or interband transitions, can be used to explain the change in the band gap energy, especially for TiO_2 nanotubes. Both interband transitions and quantum confinement should be taken into account to explain these findings.

CONCLUSION

We have successfully deposited TiO_2 thin films and TiO_2 nanotubes using ALD technology with an AAO template on Si and quartz substrates at 400 °C. The intensities of the absorption spectra of the TiO_2 thin film and the TiO_2 nanotubes are enhanced by an increase in the film and tube wall thicknesses. According to the analysis of indirect interband transitions, the absorption edges of the TiO_2 thin film for 50, 100, 200, 300, and 700 deposition cycles are 3.35, 3.35, 3.19, 3.19, and 3.19 eV, respectively. The absorption edges of the TiO_2 nanotubes for 50, 100, 200, 300, and 700 deposition cycles are 3.47, 3.43, 3.42, 3.42, and 3.32 eV, respectively. From the results of the ΔE_g analysis, the variations in the absorption edges of the TiO_2 thin film could be explained by quantum confinement. However, quantum confinement could not be used to explain the changes in the band gap energy of the TiO_2 nanotubes. According to the analysis of direct interband transitions, the absorption edges of the TiO_2 thin film and the TiO_2 nanotubes for 200, 300, and 700 cycles are, respectively, 3.64, 3.64, and 3.63 eV and 3.75, 3.72, and 3.64 eV, which could be attributed to $X_2 \rightarrow X_1$ at 3.59 eV. Moreover, the absorption edges of the TiO_2 thin film and the TiO_2 nanotubes for 50 and 100 deposition cycles are, respectively, 4.07 and 3.93 eV and 4.03 and 4.01 eV, which could be attributed to $\Gamma_{5'} \rightarrow \Gamma_1$ at 4.05 eV. However, the absorption edges increase when the film or wall thickness decreases. Therefore, in addition to considering interband transitions, quantum confinement should be included in the analysis of the absorption edges to understand the changes in the band gap energies of both TiO_2 thin films and nanotubes.

AUTHOR INFORMATION

Corresponding Author

*E-mail: chih@mail.nctu.edu.tw.

Notes

The authors declare no competing financial interest.

ACKNOWLEDGMENTS

The authors would like to thank the National Science Council of the Republic of China, Taiwan, for the financial support of this research under Contract No. NSC 98-2221-E-009-036-MY3.

REFERENCES

(1) Yang, C. J.; Chen, C.; Wu, P. W.; Shieh, J. M.; Wang, S. M.; Liang, S. W. *J. Mater. Res.* **2007**, *22*, 1064−1071.
(2) Heo, Y. W.; Norton, D. P.; Tien, L. C.; Kwon, Y.; Kang, B. S.; Ren, F.; Pearton, S. J.; LaRoche, J. R. *Mater. Sci. Eng. Rep.* **2004**, *47*, 1−47.
(3) Li, Y.; Qian, F.; Xiang, J.; Lieber, C. M. *Mater. Today* **2006**, *9*, 18−27.
(4) Iijima, S. *Nature* **1991**, *354*, 56−58.
(5) Albu, S. P.; Ghicov, A.; Macak, J. M.; Hahn, R.; Schmuki, P. *Nano Lett.* **2007**, *7*, 1286−1289.
(6) Banerjee, S.; Misra, M.; Mohapatra, S. K.; Howard, C.; Mohapatra, S. K.; Kamilla, S. K. *Nanotechnology* **2010**, *21*, 145201.
(7) Dai, Z. R.; Pan, Z. W.; Wang, Z. L. *Adv. Funct. Mater.* **2003**, *13*, 9−24.
(8) Oh, S.-L.; Choi, K.-H.; Im, J.-E.; Wang, K.-K.; Yaung, H.-Y.; Kim, K.; Kim, Y.-R. *Nanotechnology* **2011**, *22*, 275309.
(9) Rawolle, M.; Niedermeier, M. A.; Kaune, G.; Perlich, J.; Lellig, P.; Memesa, M.; Cheng, Y.-J.; Gutmann, J. S.; Müller-Buschbaum, P. *Chem. Soc. Rev.* **2012**, *41*, 5131−5142.
(10) Wang, Z.-S.; Kawauchi, H.; Kashima, T.; Arakawa, H. *Coord. Chem. Rev.* **2004**, *248*, 1381−1389.
(11) O'Regan, B.; Grätzel, M. *Nature* **1991**, *353*, 737−740.
(12) Grätzel, M. *Nature* **2001**, *414*, 338−344.
(13) Linsebigler, A. L.; Lu, G.; Yates, J. T., Jr. *Chem. Rev.* **1995**, *95*, 735−758.
(14) Mor, G. K.; Shankar, K.; Paulose, M.; Varghese, O. K.; Grimes, C. A. *Nano Lett.* **2005**, *5*, 191−195.
(15) Park, J. H.; Park, O. O.; Kim, S. *Appl. Phys. Lett.* **2006**, *89*, 163106.
(16) Liu, C. M.; Chen, C.; Cheng, H. E. *J. Electrochem. Soc.* **2011**, *158* (3), K58−K63.
(17) Liu, C. M.; Chen, C.; Cheng, H. E. *J. Electrochem. Soc.* **2012**, *159* (4), K78−K82.
(18) Chang, Y. H.; Liu, C. M.; Chen, C.; Cheng, H. E.; Lu, T. C. *J. Electrochem. Soc.* **2012**, *159* (5), K136−K140.
(19) Chang, Y. H.; Liu, C. M.; Chen, C.; Cheng, H. E. *Nanoscale Res. Lett.* **2012**, *7*, 231.
(20) Rao, N. N.; Dube, S. *Int. J. Hydrogen Energy* **1996**, *21*, 95−98.
(21) Hesabi, Z. R.; Allan, N. K.; Dahmen, K.; Garmestani, H.; El-Sayed, M. A. *ACS Appl. Mater. Interfaces* **2011**, *3*, 952−955.
(22) Lee, K. S.; Kwon, J.; Im, J. H.; Lee, C. R.; Park, N. G. *ACS Appl. Mater. Interfaces* **2012**, *4*, 4164−4168.
(23) Xie, Y.; Ali, G.; Yoo, S. H.; Oho, S. O. *ACS Appl. Mater. Interfaces* **2010**, *2*, 2910−2914.
(24) Tan, L. K.; Kumar, M. K.; An, W. W.; Gao, H. *ACS Appl. Mater. Interfaces* **2010**, *2*, 498−503.
(25) Sander, M. S.; Côté, M. J.; Gu, W.; Kile, B. M.; Tripp, C. P. *Adv. Mater.* **2004**, *16*, 2052−2057.
(26) Serpone, N.; Lawless, D.; Khairutdinov, R. *J. Phys. Chem.* **1995**, *99*, 16646−16654.
(27) Sant, P. A.; Kamat, P. V. *Phys. Chem. Chem. Phys.* **2002**, *4*, 198−203.
(28) King, D. M.; Du, X.; Cavanagh, A. S.; Weimer, A. W. *Nanotechnology* **2008**, *19*, 445401.
(29) Monticone, S.; Tufeu, R.; Kanaev, A. V.; Scolan, E.; Sanchez, C. *Appl. Surf. Sci.* **2000**, *162−163*, 565−570.
(30) Tan, L. K.; Chong, M. A. S.; Gao, H. *J. Phys. Chem. C* **2008**, *112*, 69−73.
(31) Anpo, M.; Shima, T.; Kodama, S.; Kubokawa, Y. *J. Phys. Chem.* **1987**, *91*, 4305−4310.
(32) Kormann, C.; Bahnemann, D. W.; Hoffmann, M. R. *J. Phys. Chem.* **1988**, *92*, 5196−5201.
(33) Kavan, L.; Stoto, T.; Gratzel, M.; Fitzmaurice, D.; Shklover, V. *J. Phys. Chem.* **1993**, *97*, 9493−9498.

(34) Yuwono, A. H.; Xue, J. M.; Wang, J.; Elim, H. I.; Ji, W.; Li, Y.; White, T. J. *J. Mater. Chem.* **2003**, *13*, 1475−1479.
(35) Yang, C. J.; Wang, S. M.; Liang, S. W.; Chang, Y. H.; Chen, C.; Shieh, J. M. *Appl. Phys. Lett.* **2007**, *90*, 033104.
(36) Chang, Y. H.; Liu, C. M.; Chen, C.; Cheng, H. E. *J. Electrochem. Soc.* **2012**, *159* (7), D401−D405.
(37) Alivisatos, A. P. *Science* **1996**, *271*, 933−937.
(38) Weisbuch, C.; Benisty, H.; Houdré, R. *J. Lumin.* **2000**, *85*, 271−293.
(39) Tang, H.; Prasad, K.; Sanjines, R.; Schmid, P. E.; Levy, F. *J. Appl. Phys.* **1994**, *75*, 2042−2047.
(40) Parker, R. A. *Phys. Rev.* **1961**, *124*, 1719−1722.
(41) Boudreaux, D. S.; Williams, F.; Nozik, A. J. *J. Appl. Phys.* **1980**, *51*, 2158−2163.
(42) Daude, N.; Gout, C.; Jouanin, C. *Phys. Rev. B* **1977**, *15*, 3229−3235.